Carbapenem-resistance *oprD* mutations reshape *Pseudomonas aeruginosa* host-pathogen interactions during infection

Pablo Laborda[1,*], Claudia Antonella Colque[1], Ruggero La Rosa[1,2], Søren Molin[3], Helle Krogh Johansen[1,2,4].

[1] Department of Clinical Microbiology 9301, Rigshospitalet, 2100 Copenhagen, Denmark

[2] Department of Health Technology, Technical University of Denmark, 2800 Kgs. Lyngby, Denmark

[3] The Novo Nordisk Foundation Center for Biosustainability, Technical University of Denmark, 2800 Kgs. Lyngby, Denmark

[4] Department of Clinical Medicine, Faculty of Health and Medical Sciences, University of Copenhagen, 2200 Copenhagen, Denmark

*Corresponding author: Pablo Laborda (palama@biosustain.dtu.dk)

Running title: **OprD mutations remodel *P. aeruginosa* infection**

Abstract

Antibiotic resistance is a major global health threat. While its role in reducing drug susceptibility is well established, the broader consequences of resistance mutations on bacterial physiology and behavior during infection remain poorly understood. Carbapenem-resistant *Pseudomonas aeruginosa* is considered among the highest-priority bacterial threats, with resistance commonly driven by loss-of-function mutations in the carbapenem uptake porin OprD. Here we show that such mutations can arise in clinical isolates even without prior carbapenem treatment, indicating that their effects during infection extend beyond antibiotic resistance. Consistent with this, we found that *oprD* mutants exhibit enhanced early attachment to and translocation across airway epithelial barriers in infection models, an effect maintained across strains with distinct clinical genomic backgrounds and infection dynamics. Our findings indicate that loss of OprD alters the bacterial outer membrane charge and reduces mucus entrapment, thereby facilitating epithelial barrier colonization. Overall, these results illustrate how antibiotic resistance mutations can directly shape infection dynamics, extending their impact well beyond antimicrobial susceptibility.

Introduction

Antibiotic resistance is one of the most important medical challenges of the 21st century, undermining the effectiveness of current treatments and driving higher morbidity and mortality associated with infections worldwide [1]. Gram-negative pathogens are of particular concern due to their intrinsic resistance mechanisms, low outer membrane permeability to antimicrobial agents, and ability to acquire additional resistance traits [2]. Among them, *Pseudomonas aeruginosa* stands out as a highly adaptable opportunistic pathogen capable of causing a broad spectrum of infections, especially in immunocompromised patients and individuals with chronic lung diseases such as cystic fibrosis (CF), Primary Ciliary Dyskinesia (PCD) and Chronic Obstructive Pulmonary Disease (COPD) [3–5].

In chronic infections, *P. aeruginosa* often acquires mutations that reduce the efficacy of antimicrobial agents [6,7], a phenomenon typically attributed to the selective pressure of antibiotic exposure. Resistance to carbapenems, a last resort antibiotics, is of particular concern because it severely restricts therapeutic options [8,9], placing carbapenem-resistant *P. aeruginosa* among the highest-priority bacterial threats [10]. A central determinant of carbapenem susceptibility is the outer membrane porin OprD, which mediates drug uptake of carbapenem antibiotics. Loss or alteration of OprD is among the most common mechanisms of carbapenem resistance in *P. aeruginosa* [4,11,12], and it is frequently observed in clinical isolates [6,7].

While the genetic basis of antibiotic resistance is generally well-characterized, its broader physiological consequences remain largely undiscovered. Resistance mutations can exert pleiotropic effects on bacterial envelope organization, metabolism, and virulence [13–17]. These changes may occur directly, when the altered resistance determinant is involved in core physiological processes, or indirectly through perturbation of complex regulatory networks. Notably, many of these networks are intertwined with virulence and pathogenicity pathways [18,19], suggesting that antimicrobial resistance can reshape infection dynamics in ways that extend beyond drug susceptibility.

62 Here, we show that loss-of-function mutations in *oprD* appear in clinical isolates in the
63 absence of prior carbapenem exposure, suggesting that they can provide infection-
64 related advantages beyond antibiotic resistance. Consistent with this, we observed that
65 these mutations increase *P. aeruginosa* attachment to and crossing of airway epithelial
66 barriers. Our data suggest that loss of OprD leads to a reorganization of the bacterial
67 surface and reduces mucus entrapment, thereby facilitating earlier access to the
68 epithelial surface and more rapid penetration. Together, these findings highlight how
69 examining antimicrobial resistance and bacterial physiology as interconnected traits can
70 reveal important links with direct consequences for infection outcomes.

71

72 **Results**

73 *Mutations in* oprD *appear in clinical isolates without prior carbapenem exposure but*
74 *often disappear*

75 We first investigated the clinical prevalence of *oprD* mutations in chronically infected
76 patients. For this, we examined a collection of 474 longitudinally sampled clinical
77 isolates of *P. aeruginosa* obtained from 34 chronically infected individuals with CF at the
78 Copenhagen CF Center [6]. Most mutations in *oprD* acquired during infection were
79 frameshifts, likely preventing porin production or assembly into the membrane (Figure
80 1A, Supplementary Table 1). These mutations were observed at multiple timepoints
81 throughout chronic infection. When comparing these data with carbapenem treatment
82 periods, we found that the appearance of *oprD*-mutated strains did not always coincide
83 with antibiotic exposure (Figure 1B). Importantly, carbapenem administration in these
84 patients was exclusively intravenous, as recorded in hospital treatment records, ensuring
85 that treatment histories are not confounded by undocumented oral use at different
86 timepoints. Consistent with this, meropenem Minimal Inhibitory Concentration (MIC)
87 testing showed that a substantial fraction of *oprD*-mutated isolates (26%) remained
88 susceptible according to EUCAST clinical breakpoints [20] (MIC ≤ 2; Supplementary Table
89 1), with susceptible isolates recovered both after carbapenem therapy and from patients
90 without prior exposure. Together, these observations indicate that the emergence of *oprD*

91 mutations is not solely driven by carbapenem pressure and may reflect infection-related
92 advantages beyond antibiotic resistance.

93 Despite their recurrent acquisition, *oprD* mutations were almost never maintained in the
94 infecting populations of this cohort (Figure 1B). The single case in which a mutation (3
95 nucleotide insertion) persisted throughout chronic infection (DK36 clone type) was also
96 the only one that did not cause a frameshift, and thus likely had a lower impact on protein
97 functionality. This suggests that while OprD loss may provide a selective advantage
98 during infection, the trait appears to be disadvantageous for long-term persistence in
99 chronic infection.

100

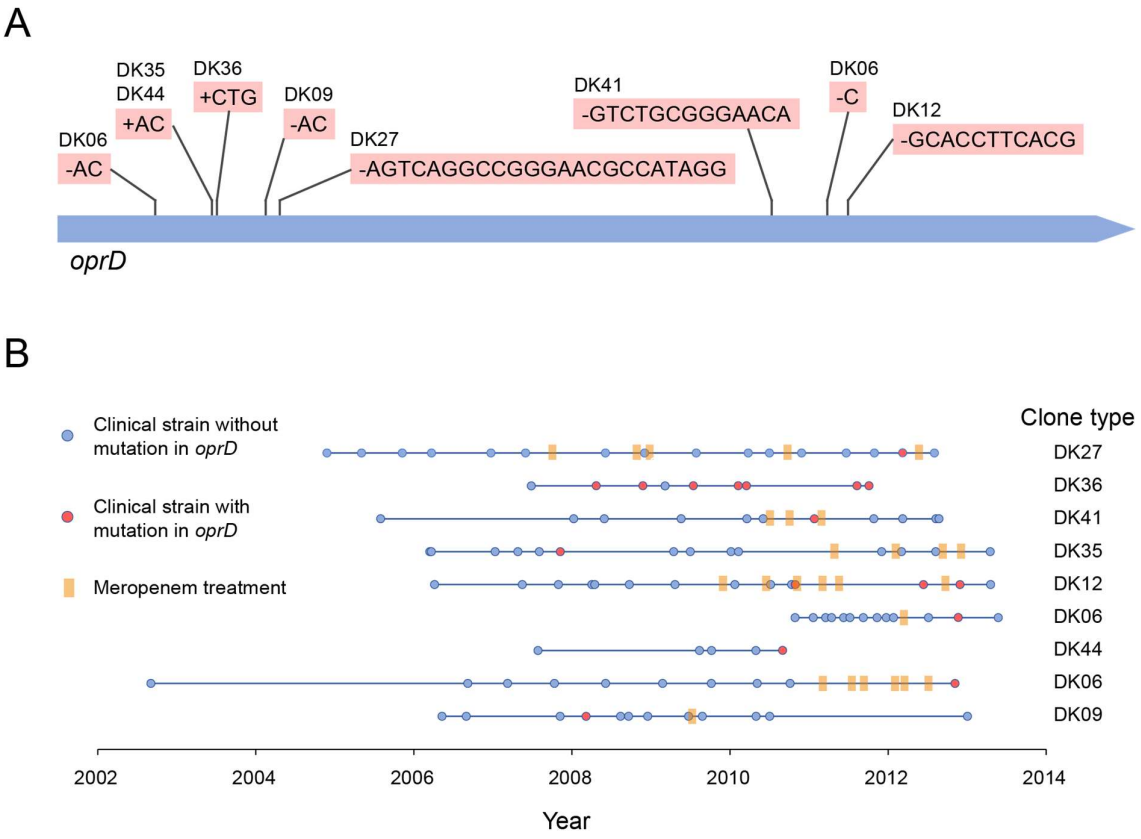

101

102 Figure 1. Characterization of *oprD* mutations in *P. aeruginosa* clinical isolates. (A) Non-
103 synonymous mutations identified in the *oprD* gene of *P. aeruginosa* clinical isolates from
104 chronically infected individuals with CF, belonging to different clone types [6]. Information
105 about the specific position of each mutation can be found in Supplementary Table 1. (B)
106 Temporal distribution of *oprD*-mutated strains during chronic infection, shown together

107 with carbapenem treatment periods of the corresponding patients. Isolates without
108 mutations are indicated by blue circles, isolates carrying *oprD* mutations by red circles,
109 and carbapenem treatment periods by orange rectangles.

110

111 *Mutations in* oprD *increase early attachment and translocation across airway epithelia*

112 The presence of OprD mutations independently of carbapenem treatment suggested that
113 OprD loss may confer infection-related advantages beyond antibiotic resistance. To
114 directly test this hypothesis, we engineered two PAO1 derivative *oprD* mutant strains
115 harboring previously identified mutations [6], to avoid the confounding effects of additional
116 mutations present in clinical genomes. One mutant carried a 13-nucleotide deletion
117 (positions 856–868) originally found in a strain with DK41 clone type (*oprD41*) that was
118 selected right after a carbapenem treatment period. The other reconstructed mutant
119 harbored a two-nucleotide (AC) deletion at positions 243–244 previously detected in a
120 clone type DK09 strain (*oprD09*), that appeared without carbapenem treatment (Figure
121 1).

122 We then compared the infection dynamics of these mutants with the wild-type PAO1
123 strain in a fully differentiated airway epithelium cultured at the air–liquid interface (ALI)
124 which exhibits barrier function and mucus production as a human airway epithelium *in*
125 *vivo* [18,21]. Following apical inoculation, bacterial growth, attachment to the epithelial cells
126 and translocation to the basolateral compartment were monitored from 1.5 to 14 hours
127 post-infection.

128 Both *oprD* mutants displayed consistently higher initial attachment and a markedly
129 increased capacity to cross the epithelial barrier compared with PAO1. CFU counts of
130 bacteria firmly attached to the epithelium (not removed by apical PBS washing) were
131 significantly higher for the mutants than for PAO1 as early as 1.5 hours post-inoculation
132 (Figure 2A, one-way ANOVA with Tukey's multiple comparisons test, $p<0.05$ for *oprD*41
133 and $p<0.001$ for *oprD*09). Mutants were also detected in the basolateral compartment by
134 10 hours post-infection, whereas wild-type PAO1 bacteria were absent at this time point,
135 and their numbers remained higher than PAO1 at 14 hours (Figure 2A, one-way ANOVA
136 with Tukey's multiple comparisons test, $p<0.0001$). Confocal microscopy analysis

137 confirmed these findings: at 10 hours, mutant bacteria were observed to be already
138 penetrating the epithelium while PAO1 cells remained largely superficial, and by 14
139 hours, mutants showed substantially deeper and more abundant epithelial penetration
140 (Figure 2B). To assess whether these infection dynamics translated into detectable
141 disruption of the epithelial barrier, we measured transepithelial electrical resistance
142 (TEER) as a general indicator of tight junction integrity and thus overall epithelial damage.
143 TEER progressively declined over the course of all infections, consistent with the large
144 epithelial barrier disruption. However, no significant differences were detected between
145 strains at the monitored timepoints (Figure 2C, two-way ANOVA with Tukey's multiple
146 comparisons test, $p>0.05$).

147 These results indicate that loss of OprD enhances *P. aeruginosa* early adhesion to and
148 translocation across the airway epithelium, although this does not affect initial overall
149 tissue disruption.

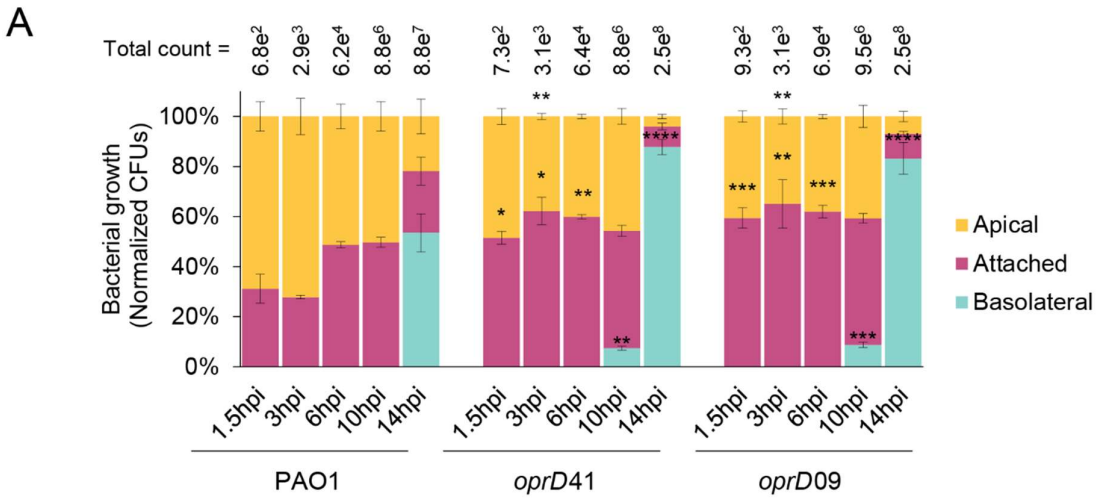
A
Total count =
6.8e2
2.9e3
6.2e4
8.8e6
8.8e7
7.3e2
3.1e3
6.4e4
8.8e6
2.5e8
9.3e2
3.1e3
6.9e4
9.5e6
2.5e8
Bacterial growth (Normalized CFUs)
100%
80%
60%
40%
20%
0%
Apical
Attached
Basolateral
1.5hpi
3hpi
6hpi
10hpi
14hpi
PAO1
oprD41
oprD09

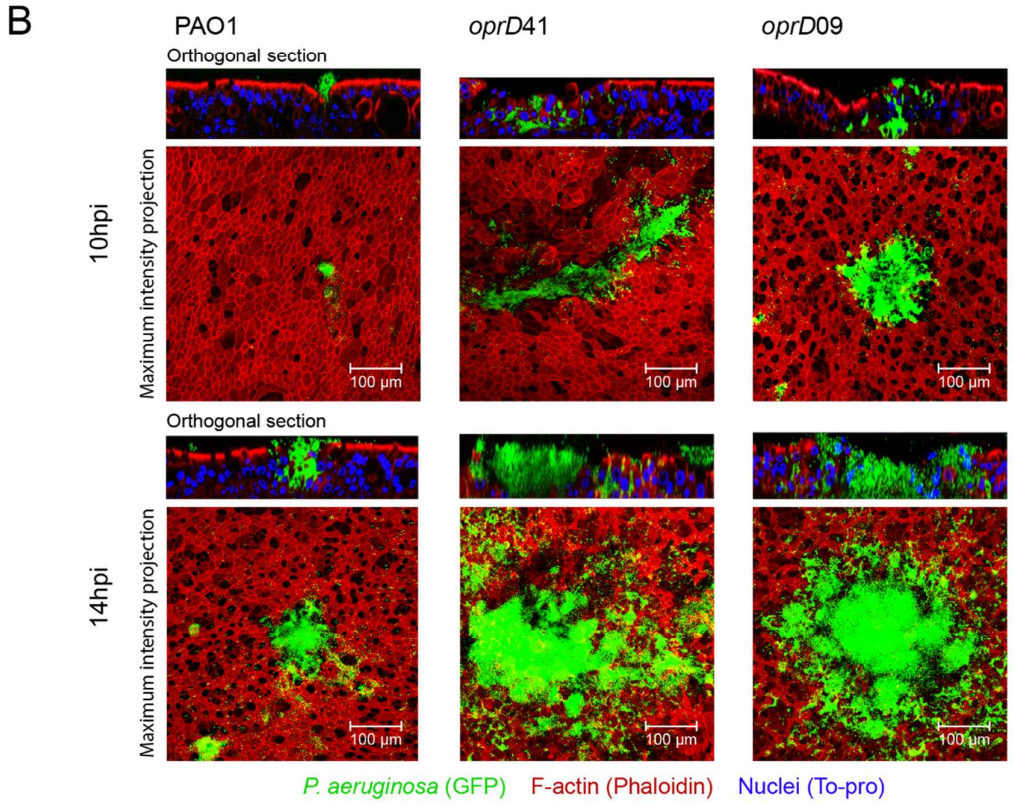
B
PAO1
oprD41
oprD09
Orthogonal section
10hpi
Maximum intensity projection
100 µm
14hpi
P. aeruginosa (GFP)
F-actin (Phaloidin)
Nuclei (To-pro)

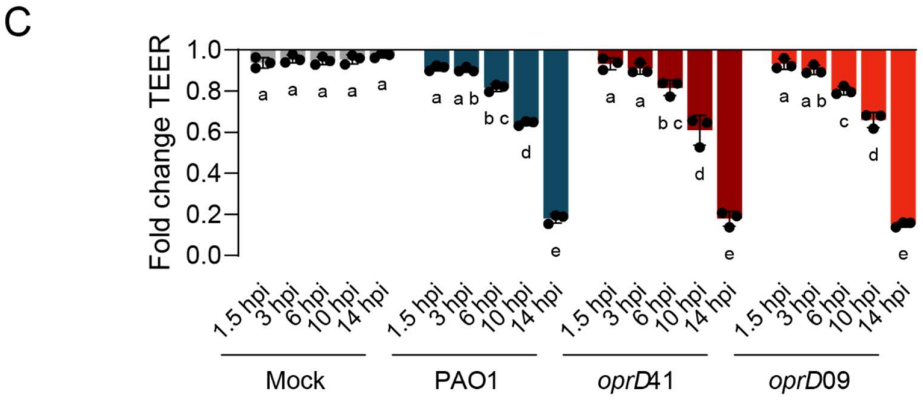
C
Fold change TEER
1.0
0.8
0.6
0.4
0.2
0.0
1.5 hpi
3 hpi
6 hpi
10 hpi
14 hpi
Mock
PAO1
oprD41
oprD09

151 Figure 2. Effects of *oprD* mutations on airway infection dynamics of *P. aeruginosa*. (A)
152 Colony-forming units (CFUs) of PAO1, *oprD*41, and *oprD*09 in the apical compartment
153 (non-firmly attached cells, in yellow), attached to the epithelium (pink), and in the
154 basolateral compartment (blue), measured from 1.5 to 14 hours post-infection in fully
155 differentiated BCi-NS1.1 ALI airway epithelial cultures. Data represent mean ± SEM from
156 three biological replicates, each with three technical replicates. Statistical significance
157 was determined by compartment and timepoint by one-way ANOVA with Tukey's multiple
158 comparisons test and is indicated as *p ≤ 0.05, **p ≤ 0.01, ***p ≤ 0.001 and
159 ****p ≤ 0.0001. (B) Confocal microscopy images of BCi-NS1.1 ALI cultures at 10- and 14
160 hours post-infection with PAO1, *oprD*41, and *oprD*09. Bacteria are shown in green (GFP),
161 epithelial F-actin in red (Phalloidin-AF555), and nuclei in blue (TO-PRO-3). Nuclei signal
162 was omitted from maximum intensity projections for image clarity. Scale bar, 100 µm.
163 Images are representative of three independent experiments. (C) Fold change in
164 transepithelial electrical resistance (TEER) of fully differentiated BCi-NS1.1 ALI airway
165 epithelial cultures left uninfected (Mock, in grey) or infected with PAO1 (blue), *oprD*41
166 (dark red), or *oprD*09 (light red), calculated at the end of the experiment (1.5 to 14 hours)
167 relative to baseline values at the beginning. Data represent mean ± SEM from three
168 biological replicates, each with three technical replicates. Statistical significance was
169 assessed by two-way ANOVA with Tukey's multiple comparisons test; connecting letters
170 indicate significant differences between groups ($p<0.05$).

171

172 *Mutations in* oprD *are associated with changes in membrane organization and adherence*
173 *to mucin*

174 To investigate the mechanisms underlying the enhanced epithelial crossing of the *oprD*
175 mutants, we performed both phenotypic screenings and transcriptomic analyses on the
176 bacterial monocultures grown in laboratory media Luria–Bertani (LB). In *in vitro* virulence
177 analyses such as pyocyanin production, protease secretion, biofilm formation, and
178 swarming motility, the mutant strains showed no significant differences from the wild-
179 type PAO1 (Supplementary Figure 1A, 1B, 1C and 1D, one-way ANOVA with Tukey's
180 multiple comparisons test, p>0.05). Likewise, RNA-seq analysis revealed no significant
181 transcriptional changes between strains (Supplementary Figure 2A and 2B), with no

genes meeting differential expression thresholds ($|\log_2$ fold change$| \geq 1$, adjusted $p < 0.05$). These results indicate that the absence of OprD does not involve a global transcriptional reorganization.

Because type III secretion (T3SS) has been described as a key determinant of epithelial colonization and penetration [22], and its expression is strongly host-induced [23], we also quantified the transcript levels of five T3SS genes representing different operons by RT-qPCR from total RNA extracted from infected ALI cultures after 14 hours of infection. Consistent with the RNA-seq data obtained in LB, no significant differences were detected between PAO1 and the *oprD* mutants (Supplementary Figure 2C), supporting that the enhanced epithelial phenotype is not due to altered T3SS expression.

We next assessed bacterial fitness in LB and synthetic cystic fibrosis sputum medium (SCFM) which mimics the nutritional composition of the CF airways [24]. Growth of the mutants was indistinguishable from PAO1 (Supplementary Figure 1E, one-way ANOVA with Tukey's multiple comparisons test, $p>0.05$), ruling out a contribution of general fitness. Antibiotic susceptibility profiling confirmed the expected increase in carbapenem resistance and additionally revealed a modest decrease in colistin susceptibility (Figure 3A, Supplementary Figure 3). Because colistin is an antimicrobial peptide that interacts with the bacterial surface, we hypothesized that OprD loss altered membrane properties.

Consistent with this hypothesis, we quantified alterations in outer membrane organization. The *oprD* mutants exhibited a significantly more negative net surface charge than PAO1 (Figure 3B, one-way ANOVA with Tukey's multiple comparisons test, $p<0.05$ for *oprD*41 and $p<0.01$ for *oprD*09), as determined by zeta potential measurements, which report on the electrostatic properties of the bacterial surface. To further assess membrane organization, we used the fluorescent probe Laurdan, which is sensitive to lipid packing and allows discrimination between changes in membrane fluidity (generalized polarization, GP) and overall probe accessibility (fluorescence intensity). Laurdan GP values remained unchanged ($GP_{PAO1} = 0.51 \pm 0.004$, $GP_{oprD41} = 0.52 \pm 0.002$, $GP_{oprD09} = 0.50 \pm 0.002$, one-way ANOVA with Tukey's multiple comparisons test, $p>0.05$), indicating that lipid order and membrane fluidity are preserved. However, total Laurdan fluorescence increased in the mutants (Figure 3C one-way ANOVA with Tukey's

213 multiple comparisons test, $p<0.05$), suggesting greater accessibility of outer membrane
214 components to external molecules, consistent with a structural reorganization of the
215 envelope.

216 We hypothesized that such alterations in surface properties could directly influence how
217 bacteria interact with the host environment. Given that mucus is a highly negatively
218 charged barrier that bacteria must overcome to establish infection [25,26], we next examined
219 mucin binding after incubating bacteria with commercially sourced mucin pre-coated
220 onto the wells of a microplate. Non-adherent cells were removed by washing, and the
221 number of bound bacteria was quantified by CFU counting. Notably, *oprD* mutants
222 showed impaired attachment compared to PAO1 (Figure 3D, one-way ANOVA with
223 Tukey's multiple comparisons test, $p<0.0001$), which may reduce their entrapment within
224 mucus and thereby facilitate earlier access to the epithelial surface and more rapid
225 penetration through the tissue.

226 These findings indicate that OprD loss primarily affects membrane properties and mucus
227 interaction, rather than global virulence regulation or bacterial fitness, providing a
228 plausible mechanistic basis for the enhanced epithelial penetration observed.

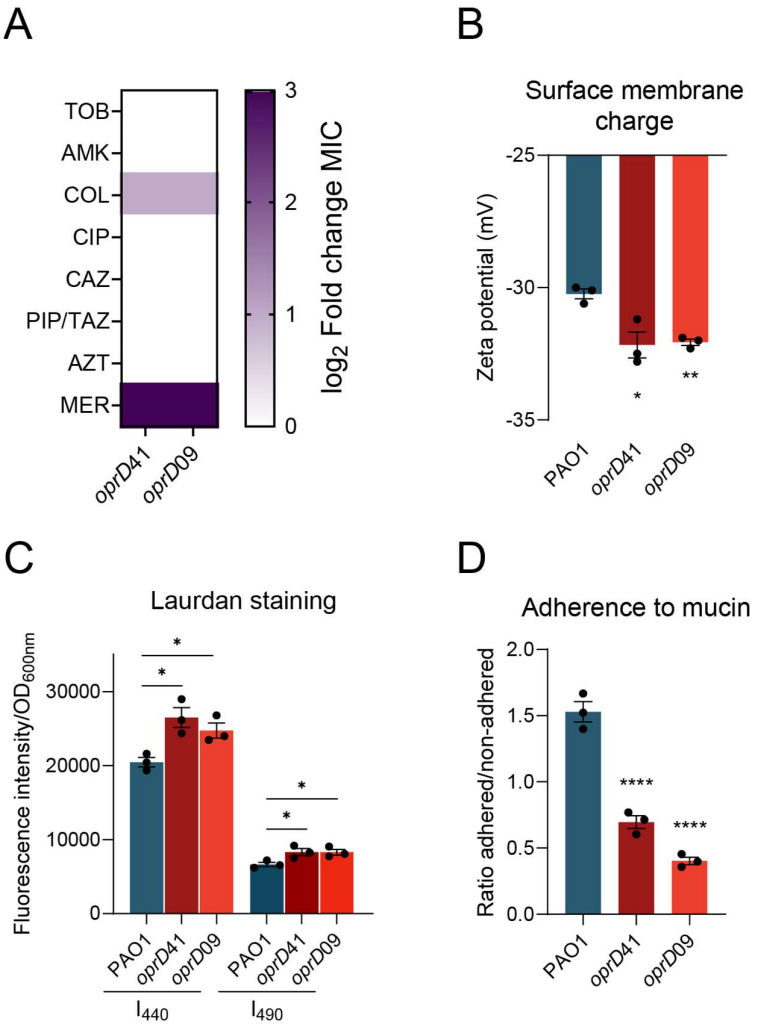

Figure 3. Phenotypic characterization of changes caused by *oprD* mutations in *P. aeruginosa*. (A) Antibiotic susceptibility of *oprD*41 and *oprD*09 relative to the parental PAO1 strain against tobramycin (TOB), amikacin (AMK), colistin (COL), ciprofloxacin (CIP), ceftazidime (CAZ), piperacillin/tazobactam (PIP/TAZ), aztreonam (AZT), and meropenem (MER). Bacterial growth data (OD_{600} values at the end of the assay across antibiotic concentrations) are provided in Supplementary Figure 2. (B) Surface charge and (C) Laurdan fluorescence intensity for PAO1 (blue), *oprD*41 (dark red), and *oprD*09 (light red). Surface charge values are shown as mean ± SEM from three biological replicates with twenty technical replicates each, whereas Laurdan fluorescence total intensity is presented as mean ± SEM from three biological replicates with three technical replicates each. Statistical significance was determined by one-way ANOVA with Tukey's multiple comparisons test and is indicated as *$p \leq 0.05$ and **$p \leq 0.01$. (D)

242 Mucin adherence of PAO1 (blue), *oprD*41 (dark red), and *oprD*09 (light red), expressed as
243 the ratio of attached to non-attached bacteria after incubation with mucin. Data
244 represent mean ± SEM from three biological replicates with three technical replicates
245 each. Statistical significance was determined by one-way ANOVA with Tukey's multiple
246 comparisons test and is indicated as ****$p \leq 0.0001$.

247

248 *Effects of* oprD *mutations on airway infection are preserved in clinical genomic*
249 *backgrounds*

250 Finally, to validate the relevance of these findings in patient-derived isolates, we tested
251 whether the infection phenotype was preserved in clinical genomic backgrounds. For
252 that, we analyzed epithelial penetration of pairs of clinical strains with or without *oprD*
253 mutation, isolated from the same sputum sample and phylogenetically related,
254 minimizing the number of confounding genetic differences (Supplementary Table 2). The
255 pairs, previously whole-genome sequenced [6], belonged to clone types DK06 (strains 305
256 and 306) and DK44 (strains 330 and 333). In DK06, strain 306 carried a deletion of a C at
257 position 927 of *oprD* and had emerged after carbapenem therapy (Figure 1), whereas
258 strain 305 retained the wild-type allele. In DK44, strain 330 harbored a two-nucleotide
259 insertion (AC) at position 184, while strain 333 carried an intact *oprD* gene; these isolates
260 were obtained from a patient who had not received prior carbapenem treatment (Figure
261 1).

262 Infections were performed in the airway epithelium ALI model, with bacterial growth,
263 attachment and translocation to the basolateral side assessed at 14 and 22 hours post-
264 inoculation. Consistent with the phenotype observed in the PAO1 background, the *oprD*
265 mutant clinical strains (306 and 330) were detected in the basolateral compartment as
266 early as 14 hours, whereas their *oprD* wild-type counterparts (305 and 333) were absent
267 at this time point, and the *oprD* mutant strains were attached to the epithelium in higher
268 numbers (Figure 4A, left panel; t-test with Holm–Šídák multiple comparisons test,
269 $p<0.05$). By 22 hours, bacteria from all strains were detectable in the basolateral
270 compartment, but *oprD* mutants remained significantly more abundant than their *oprD*
271 wild-type counterparts (Figure 4A, right panel; t-test with Holm–Šídák multiple

272 comparisons test, $p<0.05$). Confocal microscopy images at 22 hours post-infection
273 visually confirmed these quantitative results, showing deeper epithelial penetration of
274 the *oprD*-mutated strains across distinct colonization patterns (Figure 4B).

275 TEER values, measured as an indicator of epithelial barrier integrity, decreased
276 progressively over time in all strains (Figure 4C; two-way ANOVA with Tukey's multiple
277 comparisons test, $p>0.05$ between strains). However, no significant TEER reduction
278 relative to uninfected controls was observed at 14 hours post-infection for any strain
279 (Figure 4C; two-way ANOVA with Tukey's multiple comparisons test, $p>0.05$), indicating
280 that these clinical isolates are less damaging to the epithelium than the laboratory strain
281 PAO1 (Figure 2C).

282 Consistent with the observations in the PAO1 background, the *oprD* mutant clinical
283 strains also showed reduced adhesion to mucin compared with their *oprD* wild-type
284 counterparts (Figure 4D, two-way ANOVA with Tukey's multiple comparisons test,
285 $p \leq 0.0001$), suggesting that loss of OprD similarly decreases mucus entrapment in
286 clinical isolates and may contribute to their enhanced epithelial translocation.

287 Together, these findings demonstrate that the enhanced epithelial translocation
288 conferred by *oprD* mutations is preserved in clinical isolates with distinct infection
289 dynamics and virulence, underscoring the relevance of this phenotype in patient
290 infection contexts.

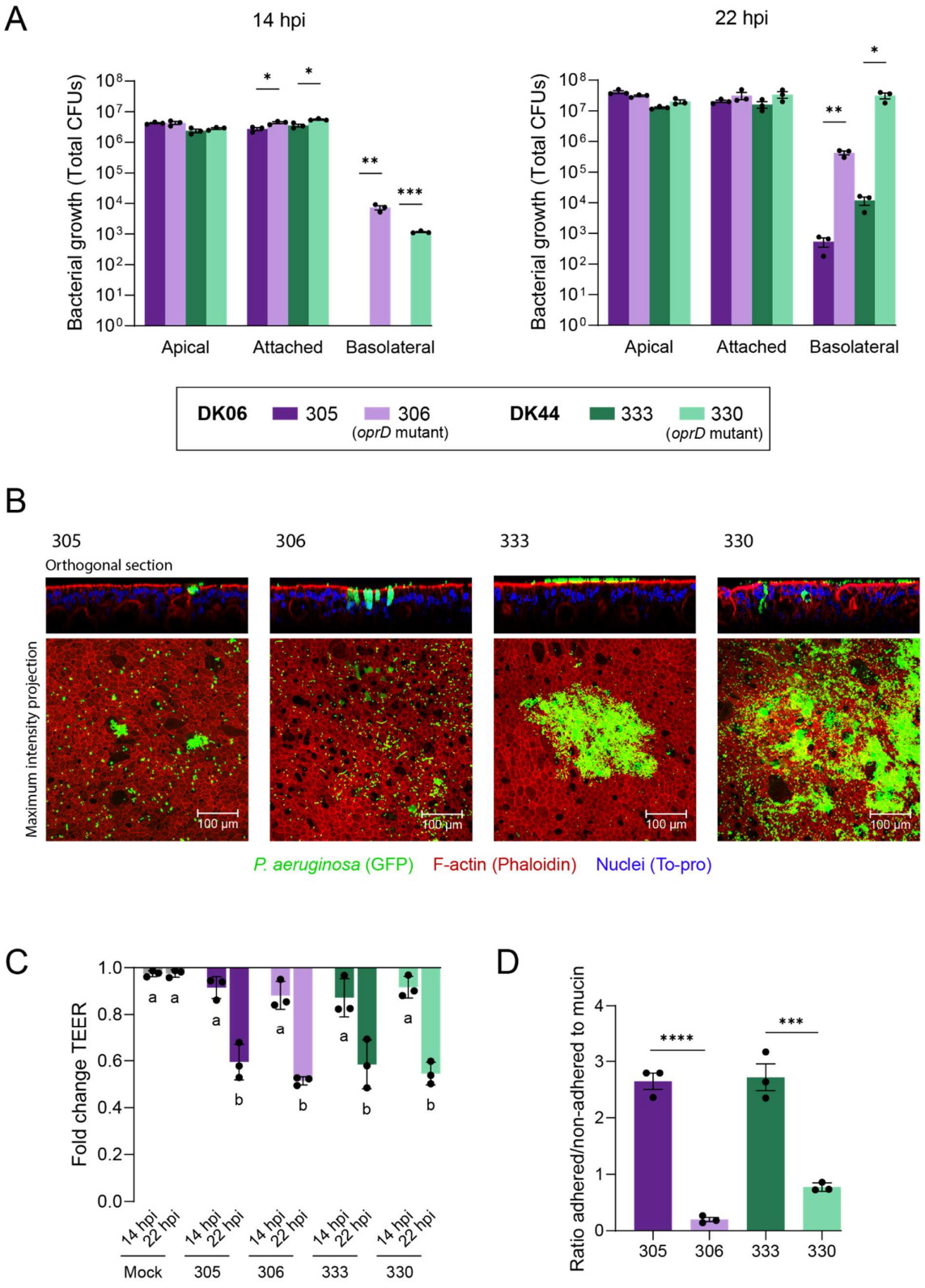

291

292 Figure 4. Effects of *oprD* mutations on airway infection dynamics of *P. aeruginosa* clinical

293 strains. (A) Colony-forming units (CFUs) of clinical strains 305 (dark purple), 306 (light

294 purple), 333 (dark green), and 330 (light green) recovered from the apical compartment
295 (non-attached cells), firmly attached to the epithelium, and from the basolateral
296 compartment at 14 (left panel) and 22 hours (right panel) post-infection in fully
297 differentiated BCi-NS1.1 ALI airway epithelial cultures. Data represent mean ± SEM from
298 three biological replicates, each performed in technical triplicates. Statistical
299 significance between strains of the same clone type was assessed by t-test with Holm–
300 Šídák multiple comparisons test and is indicated as *p ≤ 0.05, **p ≤ 0.01 and
301 ***p ≤ 0.001. (B) Confocal microscopy images of BCi-NS1.1 ALI cultures at 22 hours
302 post-infection with clinical strains 305, 306, 333, and 330. Bacteria are shown in green
303 (GFP), epithelial F-actin in red (Phalloidin-AF555), and nuclei in blue (TO-PRO-3). Nuclei
304 signal was omitted from maximum intensity projections for image clarity. Scale bar,
305 100 µm. Images are representative of three independent experiments. (C) Fold change in
306 transepithelial electrical resistance (TEER) of fully differentiated BCi-NS1.1 ALI airway
307 epithelial cultures left uninfected (Mock, in grey) or infected with clinical strains 305 (dark
308 purple), 306 (light purple), 333 (dark green) or 330 (light green), calculated at the end of
309 the experiment (14 or 22 hours) relative to the values at the beginning. Data represent
310 mean ± SEM from three biological replicates, each with three technical replicates.
311 Statistical significance was assessed by two-way ANOVA with Tukey's multiple
312 comparisons test; connecting letters indicate significant differences between groups
313 (p<0.05). (C) Mucin adherence of clinical strains 305 (dark purple), 306 (light purple), 333
314 (dark green) and 330 (light green), expressed as the ratio of attached to non-attached
315 bacteria after incubation with mucin. Data represent mean ± SEM from three biological
316 replicates with three technical replicates each. Statistical significance was determined
317 by two-way ANOVA with Tukey's multiple comparisons test and is indicated as
318 ***p ≤ 0.0005 and ****p ≤ 0.0001.

319

320 **Discussion**

321 Antibiotic resistance is typically only studied in the narrow context of drug susceptibility,
322 yet its broader effects on bacterial physiology and host interactions remain
323 underexplored. Resistance mutations can reconfigure fundamental aspects of bacterial
324 biology, thereby shaping infection outcomes in ways not directly related to antimicrobial

325 therapy. Here, we provide a clear example: loss-of-function mutations in the carbapenem
326 porin OprD in *P. aeruginosa* alter infection dynamics independently of resistance.
327 Specifically, we show that *oprD* mutants exhibit reduced mucin adhesion and enhanced
328 epithelial translocation (Figure 5).

329 This phenotype appears to arise from structural alterations of the outer membrane rather
330 than transcriptional reprogramming. Although direct genetic reversion of only the
331 membrane changes caused by OprD loss is not feasible, and chemical modulation of
332 membrane charge would also affect the host environment, the convergence of our data
333 strongly supports membrane reorganization as the most plausible driver of the observed
334 effects. This interpretation is supported by parallels with *Streptococcus pneumoniae*,
335 whose polysaccharide capsule, particularly when highly negatively charged, reduces
336 mucus-mediated clearance, facilitating transit to and colonization of the epithelial
337 surface [27]. Notably, *P. aeruginosa* has been shown to breach the airway epithelium via
338 goblet cell invasion [22], which requires overcoming entrapment within the mucin secreted
339 by these cells. This suggests that surface modifications reducing mucus entrapment may
340 represent a conserved strategy among respiratory pathogens.

341 Interestingly, we found that clinical *oprD* mutations can arise both with and without prior
342 carbapenem treatment. Notably, the clinical mutations analyzed in this study, both
343 acquired following carbapenem therapy and in patients without exposure, conferred
344 similar infection-relevant phenotypes. This observation underscores that selective
345 forces acting during infection are not limited to antibiotic exposure. Indeed, previous
346 reports have also described *oprD* mutations emerging in patients without therapy [28],
347 further supporting the idea that the selective advantage of *oprD* loss extends beyond drug
348 resistance. One possible explanation is that reduced mucin binding facilitates evasion of
349 mucociliary clearance, providing a selective advantage during airway colonization even
350 in the absence of antibiotic pressure. Importantly, we found that these infection-related
351 phenotypes were maintained across clinical strains with distinct genomic backgrounds,
352 virulence and infection dynamics, indicating that the effect of *oprD* loss is robust and not
353 restricted to a particular strain context. Since the enhanced epithelial penetration
354 observed in *oprD* mutants likely stems from an altered interaction with mucus that
355 promotes earlier contact with epithelial cells, rather than from changes in their

356 colonization strategy, the phenotype can be maintained across strains with different
357 infection dynamics. Nevertheless, we also observed that *oprD* mutations were rarely
358 maintained over time in chronic infections. This transient presence suggests an
359 evolutionary trade-off, as OprD loss facilitates short-term invasion of the airway
360 epithelium but may incur fitness costs, possibly immunological, that limit long-term
361 persistence during chronic colonization. In this sense, *oprD* mutations exemplify the
362 classic evolutionary trade-off in host-pathogen interactions: what benefits acute
363 invasion may ultimately hinder long-term persistence [29]. Still, it is unclear which other
364 selective pressures may select for *oprD* mutations.

365 Despite their limited fixation, *oprD* mutations can have clinically relevant consequences.
366 For example, it was reported that, in one CF patient, the acquisition of an *oprD* mutation
367 after carbapenem therapy coincided with a rare increase in virulence during chronic
368 infection [30]. Although concomitant mutations in the type III secretion system likely
369 contributed substantially to this phenotype, the simultaneous emergence of an *oprD*
370 mutation suggests a possible combined effect. Consistent with this, our data show that
371 the enhanced epithelial penetration associated with *oprD* loss is maintained across
372 clinical isolates with different baseline levels of virulence, as reflected by TEER
373 measurements of the performed infections, indicating that this phenotype is largely
374 independent of strain-specific virulence traits. More broadly, a recent large-scale
375 analysis found that *oprD* mutations were the strongest genomic predictors of septic
376 shock in *P. aeruginosa* infections, outperforming even classical virulence genes [31].
377 Together, these findings indicate that *oprD* mutations may shape clinical trajectories in
378 ways not captured by traditional views of resistance.

379 In addition to their impact on patient outcomes, the enhanced translocation ability of
380 *oprD* mutants may also influence bacterial dissemination. In a murine model of gut
381 infection, *oprD* mutants displayed higher fitness when bacterial recovery from the spleen
382 was used as a readout [32], consistent with our mechanistic observations of improved
383 epithelial penetration. Furthermore, in critically ill patients, a well-described gut-to-lung
384 translocation event of *P. aeruginosa* coincided with carbapenem treatment and the
385 emergence of *oprD* mutations [33]. While these mutations were originally interpreted

386 merely as genetic markers to track strain identity, our results suggest they may actively
387 promote epithelial traversal, facilitating within-host dissemination.

388 Taken together, our findings reveal that *oprD* loss-of-function mutations promote airway
389 barrier penetration, likely through alterations in outer membrane properties and mucus
390 interaction. However, their lack of stable persistence in chronic infection highlights a
391 trade-off between short-term invasiveness and long-term adaptation. More broadly, our
392 study illustrates that resistance mutations should not be viewed solely through the lens
393 of antibiotic susceptibility. Instead, their interconnection with bacterial physiology can
394 have significant implications for infection dynamics and clinical outcomes beyond the
395 reduction of drug susceptibility. Recognizing these dual roles may ultimately improve
396 how we interpret bacterial genomes in clinical microbiology and refine our predictions of
397 infection progression, with direct implications for patient management.

398

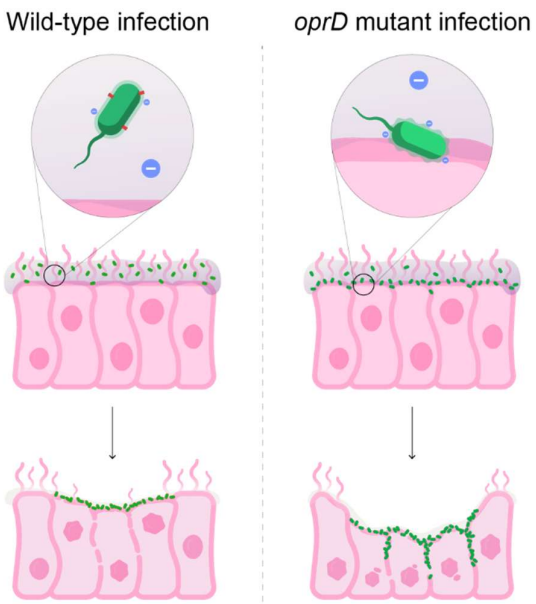

399

400 Figure 5. Schematic representation of the effects of *oprD* mutations in *P. aeruginosa*
401 infection. Loss-of-function mutations in *oprD* alter outer membrane organization and
402 increase surface negative charge. These changes likely reduce bacterial binding to
403 mucus, thereby facilitating closer contact with the epithelial surface at early timepoints.
404 This enhanced epithelial interaction promotes more efficient colonization and
405 subsequent translocation across the airway barrier.

406 **Materials and methods**

407 *Bacterial strains growth and antibiotic susceptibility testing*

408 The *P. aeruginosa* laboratory strain PAO1 was employed as the reference background for
409 constructing recombinant strains [34]. *P. aeruginosa* clinical strains used in this study were
410 previously described and whole-genome sequenced [6]. The local ethics committee at the
411 Capital Region of Denmark (Region Hovedstaden) approved the use of the
412 stored *P. aeruginosa* isolates (registration number H-21078844). Bacterial strains were
413 cultured routinely in LB medium at 37 °C under aerobic conditions.

414 Bacterial growth was monitored in a BioTek ELx808 Absorbance Microtiter Reader (BioTek
415 Instruments) at 37 °C with shaking at 250 rpm. Optical density (OD) at 600 nm was
416 recorded at 20-minutes intervals over a 24-hours period. Cultures were initiated at an
417 OD_{600} of 0.01, obtained by diluting overnight LB precultures into fresh LB or SCFM. SCFM
418 was prepared following the protocol described previously [35], excluding DNA and mucins
419 to reduce viscosity.

420 The minimum inhibitory concentrations (MICs) of ciprofloxacin, ceftazidime, tobramycin,
421 amikacin, colistin, piperacillin/tazobactam, aztreonam, and meropenem were
422 determined for multiple *P. aeruginosa* strains using the broth microdilution method in
423 Mueller–Hinton (MH) medium, following the guidelines established by the European
424 Committee on Antimicrobial Susceptibility Testing (EUCAST) [36].

425

426 *Construction of bacterial strains*

427 Genetic modifications were carried out using a CRISPR-Cas9-based recombineering
428 system with a protocol previously described [37], that is briefly described below.

429 Electrocompetent *P. aeruginosa* PAO1 cells were prepared by washing twice with 300 mM
430 sucrose, followed by electroporation with the pSH624-ssr plasmid. Transformants were
431 selected on LB-agar plates supplemented with gentamicin (50 µg/mL). Spacer
432 sequences targeting the *oprD41* mutation (Fw: 5'–GCGCGGGATGCGCACACTTTCACCT–
433 3'; Rv: 5'–AAACAGGTGAAAGTGTGCGCATCCC–3') and *oprD09* mutation (Fw: 5'–
434 GCGCGTATGAATCCGGCTTCACCCA–3'; Rv: 5'–AAACTGGGTGAAGCCGGATTCATAC–3')

435 were phosphorylated using T4 Polynucleotide Kinase (New England Biolabs) and cloned
436 into Eco31I (FastDigest, Thermo Fisher Scientific)-digested pS548-CsR vector via T4 DNA
437 ligase (Thermo Fisher Scientific), following the manufacturers' protocols.

438 To induce ssr expression, an overnight culture of PAO1 pSH624-ssr was incubated with 1
439 mM IPTG for 3 hours. Subsequently, the constructed pS548-CsR-*oprD41* and pS548-
440 CsR-*oprD09* plasmids were introduced by electroporation together with the
441 recombineering oligonucleotides containing the desired genetic modification flaked by
442 50 nucleotides upstream and downstream of its genetic context. Transformants were
443 selected on LB agar containing tetracycline (100 µg/mL), and Cas9 activity was induced
444 by adding 5 mM 3-methylbenzoate (3-mBz) into the LB-agar plate. Successful genome
445 editing was confirmed by PCR screening and Sanger sequencing of the targeted genomic
446 region.

447

448 *GFP-tagging of bacterial strains*

449 To enable visualization by confocal microscopy, *P. aeruginosa* strains were genetically
450 modified to express GFP. Tagging was achieved by conjugative transfer of the plasmid
451 pUC18T-mini-Tn7T-Gm-Tp-gfp as previously described [18,38]. The process involved a four-
452 parental mating, in which equal volumes of cultures of *Escherichia coli* DH5α/pUC18T-
453 mini-Tn7T-Gm-Tp-gfp, *E. coli* SM10(λpir)/pTNS1, *E. coli* HB101/pRK2013, and the target *P.*
454 *aeruginosa* strain were applied onto a 3-mm cellulose acetate filter placed on non-
455 selective LB agar. Plates were incubated overnight at 37 °C. Transformants were selected
456 on Pseudomonas Isolation Agar (PIA) supplemented with gentamycin (50 µg/mL).
457 Subsequently, the antibiotic resistance cassette was removed by Flp-mediated excision
458 using the plasmid pFLP2. For this step, electrocompetent *P. aeruginosa* cells from the
459 previous conjugation were prepared by two washes with 300 mM sucrose, followed by
460 electroporation with pFLP2. Transformants were selected on LB agar containing
461 carbenicillin (200 µg/mL). Plasmid curing was performed by streaking onto LB agar with
462 5% sucrose. GFP expression in the final strains was confirmed by detection of green
463 fluorescence.

464

465 *Air Liquid Interface infection model preparation*

466 BCi-NS1.1 cells [21] were employed to establish ALI-based infection systems as previously
467 described [17,18]. Cells were first expanded in standard culture flasks under humidified
468 conditions at 37 °C and 5% CO_2, using PneumaCult™-Ex Plus medium (STEMCELL
469 Technologies) according to the manufacturer's guidelines. For ALI setup, 1×10^5 cells were
470 seeded onto 1 µm pore polyester membrane inserts (Falcon) pre-coated with type I
471 collagen (Gibco). Once full confluence was achieved, the apical medium was removed,
472 and the basolateral compartment was replenished with PneumaCult™-ALI maintenance
473 medium (STEMCELL Technologies) supplemented with 4 µg/mL heparin, 480 ng/mL
474 hydrocortisone, PneumaCult™-ALI 10× supplement, and PneumaCult™-ALI maintenance
475 supplement. Cultures were maintained for 28 days at 37 °C and 5% CO_2, with media
476 replacement every 3–4 days. Epithelial polarization was monitored by regular
477 measurements of transepithelial electrical resistance (TEER) using an STX2 chopstick
478 electrode (World Precision Instruments). From day 15 onward, accumulated mucus was
479 removed weekly by rinsing the apical surface with PBS.

480

481 *Infection procedure and characterization*

482 Overnight cultures of *P. aeruginosa* were diluted in LB medium to an initial OD_{600} of 0.01
483 and incubated until reaching mid-exponential growth. One milliliter of culture was then
484 pelleted by centrifugation (4500 × g, 5 minutes), washed with PBS, and resuspended in
485 PBS to a final concentration of 1×10^5 CFU/mL. For infection, 10 µL of this suspension
486 ($\approx1\times10^3$ CFU) were applied to the apical compartment of fully differentiated BCi-NS1.1
487 ALI cultures, with 600 µL of supplemented PneumaCult™-ALI maintenance medium in the
488 basolateral chamber. Control wells received the same volume of sterile PBS. Cultures
489 were incubated at 37 °C and 5% CO_2 for the desired infection period, after which 200 µL
490 of PBS were added to the apical chamber.

491 Apical washes (200 µL) and basolateral media (600 µL) were collected for CFU counting
492 by serial dilution and plating on LB agar. To quantify adherent bacteria, the apical surface
493 was rinsed with 200 µL PBS, epithelial cells were detached using a cell scraper, and
494 resulting suspensions were serially diluted and plated.

495 For confocal microscopy, infected ALI cultures were rinsed with PBS and fixed with 4%
496 paraformaldehyde applied to both apical and basolateral chambers for 20 minutes at 4
497 °C. After three PBS washes, samples were permeabilized and blocked with PBS
498 containing 3% BSA, 1% saponin, and 1% Triton X-100 for 1 hour at room temperature.
499 Staining was performed by adding 100 µL of Phalloidin-AF555 (1:400, Invitrogen) and TO-
500 PRO-3 (1:1000, BioLegend) diluted in 3% BSA/1% saponin-PBS to the apical chamber for
501 2 hours at room temperature. Inserts were then excised, mounted on glass slides with
502 VECTASHIELD® Antifade Mounting Medium (VWR), and imaged using a Leica Stellaris 8
503 confocal microscope (40× oil objective, NA 1.3). Images were processed with LAS X
504 software v1.4.4.26810 (Leica).

505

506 *RNA preparation and RNA-sequencing*

507 Bacteria were inoculated into LB medium at an initial OD_{600} of 0.01 and cultured at 37 °C
508 with shaking at 200 rpm until reaching mid-exponential phase ($OD_{600} \approx 0.6$). Three
509 independent biological cultures were assessed for PAO1, *oprD*41, and *oprD*09. Prior to
510 RNA extraction, transcription was blocked by adding RNA Protect Bacteria solution
511 (Qiagen) following the manufacturer's protocol. Total RNA was then isolated using the
512 RNeasy Mini Kit (Qiagen) according to the supplier's instructions. RNA quality and
513 integrity were assessed using a Fragment Analyzer 2100 (Agilent Technologies). Samples
514 were run in a NovaSeq Illumina sequencer with 2x150bp configuration yielding 10 million
515 reads per sample.

516 Reads were trimmed, and low-quality reads and potential contamination from adapters
517 were removed using Trimmomatic (v0.35) tool [39]. Reads were further processed using
518 SortMeRNA tool (v2.1) [40] to remove reads generated from residual rRNA transcripts.
519 Reads were mapped against PAO1 genome (NCBI: NC_002516.2) using BWA-MEM
520 algorithm, and duplicated reads were marked using Picard tools. Reads mapping on each
521 annotated coding sequence were counted using htseq-count v0.7.2 [41] imported and
522 processed in RStudio.

523 Counts were normalized using log2-negative binomial transformation performed using
524 the rld transformation function contained in the R package DESeq2 [42] with the option

525 blind set as “true.” Normalized counts were used to evaluate whole transcriptome
526 similarities using hierarchical clustering analysis (HCA), principal component analysis
527 (PCA), and k-mean clustering. DEG analysis between transcriptomes was performed
528 using the R package DESeq2, considering statistically significant genes with a Log2(fold
529 change) ≥ |1| and an adjusted P ≤ 0.01.

530

531 *RNA extraction and quantitative RT-PCR from infected cultures*

532 Fully differentiated BCi-NS1.1 ALI cultures were infected with approximately 10^3 CFU of
533 each bacterial strain as described above. For each strain, three biological replicates were
534 performed, each consisting of two cell culture inserts pooled to increase bacterial RNA
535 yield. After 14 hours incubation at 37 °C and 5 % CO_2, transcription was stopped by
536 adding 300 µL RNAprotect Bacteria Reagent (Qiagen) per replicate. Total RNA was
537 extracted using the RNeasy Mini Kit (Qiagen) according to the manufacturer’s
538 instructions and treated with TURBO DNase (Invitrogen) to remove residual genomic
539 DNA. cDNA synthesis was performed from 10 µg of RNA with the GoScript Reverse
540 Transcription Mix (Promega). Quantitative PCR was run on a QuantStudio 5 Real-Time
541 PCR System (Applied Biosystems) using 96-well plates and GoTaq qPCR Master Mix
542 (Promega), with 100 ng cDNA per reaction. Cycling conditions were 95 °C for 10 min
543 followed by 40 cycles of 95 °C for 15 s and 60 °C for 1 min. Primers (400 nM) are listed in
544 Supplementary Table 3. Relative expression was calculated by the $2^{-\Delta\Delta CT}$ method [43] using
545 *rplU* as housekeeping reference. Data represents the mean of three biological replicates
546 with three technical replicates each.

547

548 *Protease secretion and pyocyanin production*

549 Protease secretion and pyocyanin production were measured as previously performed
550 [17].Overnight cultures of *P. aeruginosa* were adjusted to an OD_{600} of 0.01 in 10 mL of LB
551 medium and incubated for 24 hours at 37 °C in 50 mL flasks under constant 250 rpm
552 agitation. Each experiment was performed in three independent biological replicates.
553 One milliliter of each resulting culture was centrifuged (7000 × g, 5 minutes), and the

554 supernatant was sterilized by filtration through a 0.22 µm membrane. Two microliters of
555 the sterile supernatant were spotted onto 1% skim milk agar plates (prepared with 1%
556 agar), and proteolytic activity was evaluated by measuring clearing zones after 24 hours
557 of incubation at 37 °C. The same supernatant was also used for semi-quantitative
558 assessment of pyocyanin production by measuring absorbance at 690 nm in 100 µL
559 aliquots using a BioTek ELx808 Absorbance Microtiter Reader (BioTek Instruments).

560

561 *Biofilm production*

562 Biofilm production was assessed as previously described [44]. *P. aeruginosa* strains were
563 grown in Nunc™ MicroWell™ 96-Well Flat-Bottom Microplates (Thermo Fisher Scientific)
564 containing 150 µL of LB medium per well, with Nunc™ Immuno TSP Lids (Thermo Fisher
565 Scientific) replacing the standard lids. Bacteria were added at an initial OD_{600} of 0.05.
566 Plates were incubated at 37 °C for 20 hours to allow biofilm formation on the pegs. After
567 incubation, the peg lids were rinsed by immersion in a microtiter plate filled with 180 µL
568 PBS to remove non-adherent cells. Subsequently, the lids were transferred to a plate
569 containing 160 µL of 0.01% crystal violet solution for 15 minutes to stain the biofilms.
570 Following staining, the lids underwent three washes in separate PBS-filled microtiter
571 plates (180 µL per well) to eliminate excess dye. Finally, pegs were transferred to a fresh
572 plate with 180 µL of 99% ethanol to solubilize the bound crystal violet. The ethanol
573 solution was then used to quantify biofilm biomass by measuring absorbance at 590 nm
574 in a BioTek ELx808 Absorbance Microtiter Reader (BioTek Instruments).

575

576 *Motility assay*

577 Swarming motility was assessed using Petri dishes containing 25 mL of a defined medium
578 composed of 0.5% casamino acids, 0.5% Bacto agar, 0.5% filtered glucose, 3.3 mM
579 K_2HPO_4, and 3 mM $MgSO_4$, as previously performed [45]. Four microliters of *P. aeruginosa*
580 cultures adjusted to an OD_{600} of 1.0 were spotted onto the center of each plate. Plates
581 were incubated at 37 °C for 17 hours. Experiments included three technical replicates per

582 strain. Swarming areas were quantified by analyzing photographic images with ImageJ
583 software, measuring the surface area (cm^2) covered by bacterial spread.

584

585 *Membrane properties determination*

586 Zeta potential measurements of *P. aeruginosa* strains were performed using a Zetasizer
587 NANO-ZS (Malvern Instruments) equipped with a universal dip cell (ZEN1002). Overnight
588 cultures were washed once with ultrapure water to remove residual medium and salts,
589 then adjusted to an OD_{600} of 1. Measurements were obtained from three independent
590 biological replicates, each comprising 30 readings. Electrophoretic mobility values were
591 converted to zeta potentials using the Smoluchowski equation.

592 Membrane fluidity was assessed via Laurdan staining. Washed bacterial suspensions at
593 OD_{600} = 1 in PBS were incubated with 2.5 μM Laurdan dye for 60 minutes at room
594 temperature in the dark. 150 μL of samples and blanks were aliquoted into Nunc™ 96-
595 Well Optical-Bottom black microplates (Thermo Fisher Scientific) with three technical
596 replicates each. Fluorescence was measured at emission wavelengths of 440 and 490
597 nm upon excitation at 350 nm in a BioTek ELx808 Absorbance Microtiter Reader (BioTek
598 Instruments). Laurdan GP values were calculated using the formula:
599 $GP=(I_{440}-I_{490})/(I_{440}+I_{490})$, where I_{440} and I_{490} represent fluorescence intensities at 440 nm and
600 490 nm, respectively.

601

602 *Bacterial mucin adhesion assay*

603 Adhesion assays were conducted as previously performed [46] with minor modifications.
604 Wells of Nunc™ MicroWell™ 96-Well Flat-Bottom Microplate (Thermo Fisher Scientific)
605 were coated with 200 μL of porcine mucin (type II, Sigma-Aldrich, M2378) solution (10
606 μg/mL in PBS), while control wells received 200 μL of PBS. Plates were incubated at 37 °C
607 for 18 hours prior to the assay. Overnight bacterial cultures were washed and diluted in
608 PBS to a final concentration of 5×10^7 CFU/mL. PBS was aspirated from mucin-coated and
609 control wells, which were then inoculated in triplicate with 100 μL of the bacterial
610 suspension ($\approx5\times10^6$ CFU). Plates were incubated for 30 minutes at 37 °C to allow

611 bacterial adhesion. After incubation, the supernatant was removed, and wells were
612 washed five times with 200 μL PBS to eliminate non-attached cells. The wash solutions
613 were plated in serial dilutions to quantify non-attached bacteria. To detach adherent
614 bacteria along with mucin, 200 μL of 1% (v/v) Triton X-100 in PBS was added to each well
615 and incubated at room temperature for 30 minutes. Serial dilutions of the resulting
616 suspensions were plated to determine CFUs of adhered bacteria. Adhesion efficiency
617 was expressed as the ratio of adhered to non-adhered bacteria. All assays were
618 performed in three biological replicates.

619

620 *Statistical analysis*

621 All statistical analyses were performed with GraphPad Prism version 10.3.1 (GraphPad
622 Software). Depending on the experimental design, differences among groups were
623 assessed using ordinary one-way ANOVA or two-way ANOVA followed by Tukey's post
624 hoc test for multiple comparisons, or by unpaired *t*-tests with Holm–Šídák correction for
625 multiple comparisons. A p-value <0.05 was considered indicative of statistical
626 significance.

627

628 *Data availability*

629 All data supporting the findings of this study are available within the paper, its
630 Supplementary Materials, and Supplementary Data files. Raw sequencing data have
631 been deposited in the NCBI Sequence Read Archive (SRA) under BioProject accession
632 number PRJNA1346407. Source data are provided with this paper.

Acknowledgements

We thank the Infection Microbiology group for their insightful comments and discussion. The Basal Cell Immortalized Non-Smoker 1.1 (BCi-NS1.1) cell line was a gift from Professor Ronald G. Cristal (Weil Cornell Medical College, New York, USA). This research was funded by the "Novo Nordisk Foundation Center for Biosustainability (CfB)" grant number NNF10CC1016517 and by the Challenge Grant NNF19OC0056411 to H.K.J. from The Novo Nordisk Foundation. P.L. is the recipient of an ERS/EU RESPIRE4 Marie Skłodowska-Curie Postdoctoral Research Fellowship (Ref. nr: R4202305-01047; this project has received funding from the European Respiratory Society and the European Union's H2020 research and innovation programme under the Marie Skłodowska-Curie grant agreement No 847462).

Author contributions

PL designed the study and performed the experimental work. CAC performed the bioinformatic analysis of transcriptomic data. CAC, RLR, HKJ and SM participated in the design of the study. All authors participated in writing the manuscript and approved the submitted version.

Conflict of interest

The authors declare to have no conflict of interest.

References

1. Murray, C. J. *et al.* Global burden of bacterial antimicrobial resistance in 2019: a systematic analysis. *The Lancet* **399**, 629–655 (2022).

2. Macesic, N., Uhlemann, A. C. & Peleg, A. Y. Multidrug-resistant Gram-negative bacterial infections. *The Lancet* **405**, 257–272 (2025).

3. Laborda, P., Sanz-García, F., Hernando-Amado, S. & Martínez, J. L. Pseudomonas aeruginosa: an antibiotic resilient pathogen with environmental origin. *Curr Opin Microbiol* **64**, 125–132 (2021).

4. Laborda, P., Hernando-Amado, S., Martínez, J. L. & Sanz-García, F. Antibiotic Resistance in Pseudomonas. *Adv Exp Med Biol* **1386**, 117–143 (2022).

5. Qin, S. *et al.* Pseudomonas aeruginosa: pathogenesis, virulence factors, antibiotic resistance, interaction with host, technology advances and emerging therapeutics. *Signal Transduct Target Ther* **7**, 1–27 (2022).

6. Marvig, R. L., Sommer, L. M., Molin, S. & Johansen, H. K. Convergent evolution and adaptation of Pseudomonas aeruginosa within patients with cystic fibrosis. *Nat Genet* **47**, 57–64 (2015).

7. Weimann, A. *et al.* Evolution and host-specific adaptation of Pseudomonas aeruginosa. *Science (1979)* **385**, eadi0908 (2024).

8. World Health Organization. *WHO Bacterial Priority Pathogens List, 2024: Bacterial Pathogens of Public Health Importance, to Guide Research, Development, and Strategies to Prevent and Control Antimicrobial Resistance*. (2024).

9. Canton, R., Doi, Y. & Simner, P. J. Treatment of carbapenem-resistant Pseudomonas aeruginosa infections: a case for cefiderocol. *Expert Rev Anti Infect Ther* **20**, 1077–1094 (2022).

10. Sati, H. *et al.* The WHO Bacterial Priority Pathogens List 2024: a prioritisation study to guide research, development, and public health strategies against antimicrobial resistance. *Lancet Infect Dis* **25**, 1033–1043 (2025).

11. Darby, E. M. *et al.* Molecular mechanisms of antibiotic resistance revisited. *Nat Rev Microbiol* **21**, 280–295 (2022).

12. Wu, W., Huang, J. & Xu, Z. Antibiotic influx and efflux in Pseudomonas aeruginosa: Regulation and therapeutic implications. *Microb Biotechnol* **17**, e14487 (2024).

13. Blanco, P. *et al.* Bacterial Multidrug Efflux Pumps: Much More Than Antibiotic Resistance Determinants. *Microorganisms* **4**, 14 (2016).

686 14. Laborda, P., Gil-Gil, T., Martínez, J. L. & Hernando-Amado, S. Preserving the
687 efficacy of antibiotics to tackle antibiotic resistance. *Microb Biotechnol* **17**,
688 e14528 (2024).

689 15. Sanz-García, F. *et al.* Translating eco-evolutionary biology into therapy to tackle
690 antibiotic resistance. *Nat Rev Microbiol* **21**, 671–685 (2023).

691 16. Kong, K. F. *et al.* Pseudomonas aeruginosa AmpR is a global transcriptional factor
692 that regulates expression of AmpC and PoxB β-lactamases, proteases, quorum
693 sensing, and other virulence factors. *Antimicrob Agents Chemother* **49**, 4567–
694 4575 (2005).

695 17. Goltermann, L. *et al.* Macrolide resistance through uL4 and uL22 ribosomal
696 mutations in Pseudomonas aeruginosa. *Nat Commun* **15**, 8906 (2024).

697 18. Laborda, P. *et al.* Mutations in the efflux pump regulator MexZ shift tissue
698 colonization by Pseudomonas aeruginosa to a state of antibiotic tolerance. *Nat*
699 *Commun* **15**, 2584 (2024).

700 19. Laborda, P., Molin, S., Johansen, H. K., Martínez, J. L. & Hernando-Amado, S. Role
701 of bacterial multidrug efflux pumps during infection. *World J Microbiol Biotechnol*
702 **40**, 226 (2024).

703 20. European Committee on Antimicrobial Susceptibility Testing (EUCAST).
704 Breakpoint tables for interpretation of MICs and zone diameters. Version 15.0.
705 (2025).

706 21. Walters, M. S. *et al.* Generation of a human airway epithelium derived basal cell
707 line with multipotent differentiation capacity. *Respir Res* **14**, 135 (2013).

708 22. Leoni Swart, A. *et al.* Pseudomonas aeruginosa breaches respiratory epithelia
709 through goblet cell invasion in a microtissue model. *Nat Microbiol* **9**, 1725–1737
710 (2024).

711 23. Dasgupta, N., Ashare, A., Hunninghake, G. W. & Yahr, T. L. Transcriptional
712 Induction of the Pseudomonas aeruginosa Type III Secretion System by Low Ca2+
713 and Host Cell Contact Proceeds through Two Distinct Signaling Pathways. *Infect*
714 *Immun* **74**, 3334 (2006).

715 24. Turner, K. H., Wessel, A. K., Palmer, G. C., Murray, J. L. & Whiteley, M. Essential
716 genome of Pseudomonas aeruginosa in cystic fibrosis sputum. *Proc Natl Acad*
717 *Sci U S A* **112**, 4110–4115 (2015).

718 25. Sheng, Y. H. & Hasnain, S. Z. Mucus and Mucins: The Underappreciated Host
719 Defence System. *Front Cell Infect Microbiol* **12**, 856962 (2022).

720 26. Linden, S. K., Sutton, P., Karlsson, N. G., Korolik, V. & McGuckin, M. A. Mucins in
721 the mucosal barrier to infection. *Mucosal Immunol* **1**, 183–197 (2008).

722 27. Nelson, A. L. *et al.* Capsule Enhances Pneumococcal Colonization by Limiting
723 Mucus-Mediated Clearance. *Infect Immun* **75**, 83 (2006).

724 28. Wolter, D. J. *et al.* Emergence of carbapenem resistance in Pseudomonas
725 aeruginosa isolates from a patient with cystic fibrosis in the absence of
726 carbapenem therapy. *Clinical Infectious Diseases* **46**, e137-41 (2008).

727 29. La Rosa, R., Molin, S. & Johansen, H. K. Pseudomonas aeruginosa: persistence
728 beyond antibiotic resistance. *Trends Microbiol* **33**, 1076–1084 (2025).

729 30. Jorth, P. *et al.* Cystic fibrosis lung function decline after within-host evolution
730 increases virulence of infecting pseudomonas aeruginosa. *Am J Respir Crit Care*
731 *Med* **203**, 637–640 (2021).

732 31. Valik, J. K. *et al.* Genomic virulence markers are associated with severe outcomes
733 in patients with Pseudomonas aeruginosa bloodstream infection.
734 *Communications Medicine* **4**, 264 (2024).

735 32. Skurnik, D. *et al.* Enhanced in vivo fitness of carbapenem-resistant oprD mutants
736 of Pseudomonas aeruginosa revealed through high-throughput sequencing. *Proc*
737 *Natl Acad Sci U S A* **110**, 20747–20752 (2013).

738 33. Wheatley, R. M. *et al.* Gut to lung translocation and antibiotic mediated selection
739 shape the dynamics of Pseudomonas aeruginosa in an ICU patient. *Nat Commun*
740 **13**, 6523 (2022).

741 34. Stover, C. K. *et al.* Complete genome sequence of Pseudomonas aeruginosa
742 PAO1, an opportunistic pathogen. *Nature* **406**, 959–964 (2000).

743 35. Turner, K. H., Wessel, A. K., Palmer, G. C., Murray, J. L. & Whiteley, M. Essential
744 genome of Pseudomonas aeruginosa in cystic fibrosis sputum. *Proc Natl Acad*
745 *Sci U S A* **112**, 4110–4115 (2015).

746 36. European Committee on Antimicrobial Susceptibility Testing (EUCAST). *EUCAST*
747 *Reading Guide for Broth Microdilution - Version 5.0*. (2024).

748 37. Pankratz, D. *et al.* An expanded CRISPR–Cas9-assisted recombineering toolkit for
749 engineering genetically intractable Pseudomonas aeruginosa isolates. *Nat Protoc*
750 **18**, 3253–3288 (2023).

751 38. Choi, K. H. & Schweizer, H. P. mini-Tn7 insertion in bacteria with single attTn7
752 sites: Example Pseudomonas aeruginosa. *Nat Protoc* **1**, 153–161 (2006).

753 39. Bolger, A. M., Lohse, M. & Usadel, B. Trimmomatic: A flexible trimmer for Illumina
754 sequence data. *Bioinformatics* **30**, 2114–2120 (2014).

40. Kopylova, E., Noé, L. & Touzet, H. SortMeRNA: Fast and accurate filtering of ribosomal RNAs in metatranscriptomic data. *Bioinformatics* **28**, 3211–3217 (2012).

41. Anders, S. *et al.* Count-based differential expression analysis of RNA sequencing data using R and Bioconductor. *Nat Protoc* **8**, 1765–1786 (2013).

42. Love, M. I., Huber, W. & Anders, S. Moderated estimation of fold change and dispersion for RNA-seq data with DESeq2. *Genome Biol* **15**, 550 (2014).

43. Pfaffl, M. W. A new mathematical model for relative quantification in real-time RT-PCR. *Nucleic Acids Res* **29**, e45 (2001).

44. Bartell, J. A. *et al.* Evolutionary highways to persistent bacterial infection. *Nat Commun* **10**, 629 (2019).

45. Muñoz-Cazalla, A., Martínez, J. L. & Laborda, P. Crosstalk between Pseudomonas aeruginosa antibiotic resistance and virulence mediated by phenylethylamine. *Microb Biotechnol* **16**, 1492–1504 (2023).

46. Herrmann, C., Lingner, M., Herrmann, S., Brockhausen, I. & Tümmler, B. Mucin adhesion of serial cystic fibrosis airways Pseudomonas aeruginosa isolates. *Front Cell Infect Microbiol* **14**, 1448104 (2024).